Research Square

Preprints are preliminary reports that have not undergone peer review.
They should not be considered conclusive, used to inform clinical practice,
or referenced by the media as validated information.

Chirality-Dependent Sensing of Lung-Cancer-Associated Volatile Organic Compounds on Ag-Functionalized Single-Walled Carbon Nanotubes: A DFT Investigation

Muhammad Yaseen
University of Peshawar
Shehroz Abdullah
Islamia College University
Suhrab Khan
Islamia College University
Faizan Ahmad Khan
Islamia College University
Iqra Abdullah
CECOS University
Muhammad Asif
drmuhammadasif@cuilahore.edu.pk

COMSATS University Islamabad
Arslan Ahmad
Islamia University of Bahawalpur
Waqar Ahmad
Abdul Wali Khan University Mardan
Inzimam Ul Haq
Islamia College University
Anila Asif
COMSATS University Islamabad

Research Article

Keywords: Ag-functionalized carbon nanotubes, Volatile organic compounds, Breath analysis, Gas sensors, Chirality-dependent sensing

Posted Date: November 10th, 2026

DOI: https://doi.org/10.21203/rs.3.rs-11183336/v1

License: This work is licensed under a Creative Commons Attribution 4.0 International License.
Read Full License

Additional Declarations: No competing interests reported.

Chirality-Dependent Sensing of Lung-Cancer-Associated Volatile Organic Compounds on Ag-Functionalized Single-Walled Carbon Nanotubes: A DFT Investigation

[a] Muhammad Yaseen, [b,*] Shehroz Abdullah, [b] Suhrab Khan, [b] Faizan Ahmad Khan, [c] Iqra Abdullah [d,*] Muhammad Asif, [e] Arslan Ahmad, [f] Waqar Ahmad, [b] Inzimam Ul Haq, [g] Anila Asif

[a] Department of Physics, University of Peshawar, Pakistan.

[b] Material Modeling Lab, Department of Physics, Islamia College Peshawar 2500, Pakistan.

[c] Cecos University of IT and Emerging Sciences Hayatabad Peshawar, Khyber Pakhtunkhwa, Pakistan.

[d] Department of Physics, COMSATS University Islamabad, Lahore, 54000, Pakistan.

[e] Institute of Physics, Baghdad ul Jaded campus, Islamia University Bahawalpur Pakistan.

[f] Department of Biochemistry, Abdul Wali Khan University, Mardan, Pakistan.

[g] Interdisciplinary Research Centre in Biomedical Materials (IRCBM), COMSATS University Islamabad, Lahore, 54000, Pakistan.

Corresponding Authors Emails:

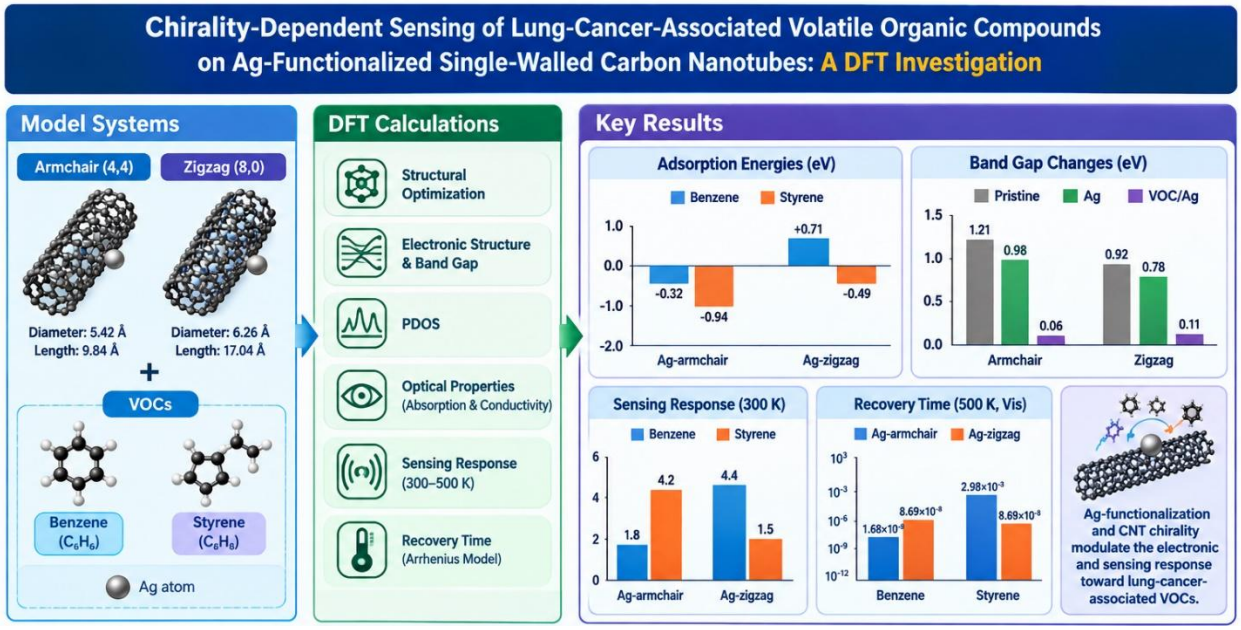
Dr. Muhammad Asif: drmuhammadasif@cuilahore.edu.pk

Shehroz Abdullah: shehroz.abdullah0300@gmail.com

Abstract

Theoretical investigation of volatile organic compounds (VOCs) using nanostructured sensing materials provides a useful approach for identifying materials with potentially distinguishable electronic responses. In this work, density functional theory calculations were employed to investigate the chirality-dependent interaction of benzene (C_6H_6) and styrene (C_8H_8) with Ag-functionalized single-walled carbon nanotubes (SWCNTs). Armchair and zigzag CNT configurations were examined before and after Ag functionalization and VOC adsorption.

Structural, electronic, projected density-of-states, optical, sensing-response, and Arrhenius-estimated recovery-time properties were analyzed. The calculated adsorption energies show different interaction characteristics for the two CNT configurations, with benzene exhibiting a positive adsorption energy on the Ag-zigzag model (+0.71 eV), whereas styrene shows exothermic adsorption on both configurations, with the strongest interaction obtained for Ag-armchair (−0.94 eV). VOC adsorption also modifies the calculated band gaps and electronic states near the Fermi level, indicating chirality-dependent electronic responses. Optical calculations reveal changes in the absorption coefficient and optical conductivity following Ag functionalization and VOC adsorption. The theoretical sensing response was evaluated over 300–500 K, while recovery times were estimated using an Arrhenius-type model. Overall, the results demonstrate that Ag functionalization and CNT chirality can modify the predicted response toward the investigated VOCs. These findings provide a theoretical basis for further experimental investigation of chirality-dependent CNT sensing platforms for lung-cancer-associated breath VOCs



Keywords: Ag-functionalized carbon nanotubes; Volatile organic compounds; Breath analysis; Gas sensors; Chirality-dependent sensing.

1. Introduction

Lung cancer is still one of the most problematic cancers globally as it is the second most prevalent cancer and the leading cause of cancer-related mortality in the world [1–3]. An estimated 1.8 million deaths occurred worldwide in 2020 due to the disease alone and prognosis is highly influenced by diagnosis. The lack of symptoms and the difficulty of diagnosis with low-dose computed tomography, chest radiography and sputum cytology highlight the need for alternative non-invasive tests that are sensitive and inexpensive to evaluate lung cancer screening [4,5]. Lung cancer is usually diagnosed at a later disease stage with a large proportion of advanced disease that cannot be cured [6]. This diagnostic discriminant has been a driver for research that has resulted in novel detection modalities capable of diagnosing the disease prior to onset of clinical symptoms. Lung cancer and other physiological or environmental processes can be associated with changes in the composition of exhaled volatile organic compounds (VOCs). More than 200 VOCs have been investigated as potential breath biomarkers, although their concentrations can be influenced by smoking, environmental exposure, metabolism, sampling conditions, and other clinical factors. Benzene and styrene are among the VOCs that have been investigated in relation to lung cancer and therefore provide relevant model analytes for theoretical gas-sensing studies [7–9]. Breath contains a complex mixture of volatile organic compounds (VOCs), some of which have been investigated as potential biomarkers associated with disease states [10]. Over 200 VOCs have been detected in human exhalations, including a number that are markers for metabolic changes correlated with malignant transformation [11,12]. Of these aromatic compounds, benzene (C_6H_6) and styrene (C_8H_8) are among the VOCs that have been investigated in exhaled-breath studies of lung cancer and therefore represent relevant model analytes for theoretical sensing investigations [13–15]. Phillips et al. reported that styrene is one of the most likely VOCs to be detected in the breath of lung cancer patients, and that benzene has also been found in multiple independent studies to be a discriminatory biomarker of lung cancer. This analysis of exhaled biomarkers, in a quantitative fashion, could be a useful tool in theoretical sensing potential if highly sensitive and highly selective sensing platforms can be developed capable of detecting trace levels in the complex breath matrix. Very high surface-to-volume ratio, great electrical conductivity, and high mechanical strength are among the properties of carbon nanotubes (CNTs) that have caught

considerable interest as material for sensing applications [17-19]. After first being discovered in 1991 by Iijima, CNTs have been widely studied for various applications such as Nano electronics and biomedical devices [17]. Because of their one-dimensional structure and their unique electronic properties, they are especially promising materials for gas sensing, since the events of adsorption of molecules in this gas will directly translate to a measurable change in the electrical resistance or optical response [20,21]. But due to some inherent limitations, such as insolubility, high hydrophobicity, low sensitivity, and low selectivity, pristine CNTs are not used practically for gas sensor applications [22,23]. Such restrictions are due to the chemically inert sp2 hybridized carbon lattice which has weak van der Waals interaction with most of the gas molecules [24,25]. The introduction of dopants (TM) to the CNTs changes the local electronic structure, leading to hybridized electronic states in the vicinity of the Fermi level and stronger adsorbate–substrate interactions as well as stronger electronic responses. Previous theoretical studies have been done on the metal-doped CNT system for VOC sensing cases such as Pt doped [26], Ni doped [13], Rh doped [27], Ir doped [28] and Pd doped [29]. Newly reported Ni-doped SWCNTs have a better affinity for benzene, styrene, isoprene and/or 1-hexene than pristine CNTs, which suggests a possible role for transition metal doping as a lung cancer biomarker [13]. Likewise, Aasi et al. demonstrated that certain kinds of SWCNTs population with platinum-group metals (PGMs) have the potential to be useful in toluene detection as nano sensors with the adsorption energies and the charge transfer characteristics desirable for practical sensing use [30]. In the case of Rh-doped CNTs, significant conductivity changes were observed upon adsorption and exposure to benzene and aniline, with this change being favorable, while the conductivity change when CO_2 is the adsorbent was not observed [27]. Also, Ir-doped CNTs are seen to possess strong adsorption towards aniline and o-toluidine [28]. More specifically Silver (Ag) is also interesting because it can be used as a dopant due to its excellent electrical conductivity, catalytic activities and availability in comparison to the other Platinum Group Metals [31]. In the experimental gas sensing platform, it has been shown that the sensitivity of CNTs can be improved by attaching silver nanoparticles that are capable of boosting the response when gases containing different analytes are sensed [31]. It is reported that the conductivity and gas sensing performance of CNT based gas sensors at room temperature can be greatly improved by decorating with Ag nanocrystal [31]. This phenomenon has been studied theoretically, and Ag doped CNTs have been studied for detection of formaldehyde [32] and furan [33] whereby Ag functionalization has been seen to

enhance the adsorption properties of CNTs. Yuksel et al. showed that SWCNTs doped with Pd, Ag, and Rh can also be used to adsorb and detect the molecules furan at room temperature and found that Ag-functionalized CNTs have an adsorption characteristic which is favorable to the furan adsorption [33]. The chirality-dependent electronic properties of CNTs are well established but the anisotropic nature of the adsorption (the armchair and zigzag geometries have radically different properties) is broadly unexplored despite this. The use of first-principles calculations to identify and explore properties of novel materials has been applied many times recently, and has been shown in the literature. Abdullah et al. have demonstrated that DFT calculations can be used to accurately predict the optoelectronic and photocatalytic properties of novel monolayers of $InAg(PSe_3)_2$ [34], Janus SnSSe [35] and $GaAg(PSe_3)_2$ [36]. The results of these investigations exemplify the case of the DFT to account for the rational design of functional materials for desired applications. In this work, one will make an effort to overcome the above-mentioned gap in literature by systematically researching the effects of anisotropic behavior of Ag-doped SWCNTs on the theoretical sensing of lung-cancer-associated VOCs. The structural, electronic and optical properties of the armchair and zigzag Ag-SWCNTs are investigated before and after the adsorption of benzene and styrene, using DFT calculations. The specific objectives of this work are (i) to calculate the adsorption energies and adsorption geometry of benzene and styrene molecules on both armchair and zigzag SWCNTs with different Ag-functionalization configurations (ii) to study the band structure and projected density of states of all of the systems to understand the electronic modification that occurs as a result of the doping and adsorption; (iii) to calculate the optical properties - the absorption coefficient and the optical conductivity - of all of the systems; and (iv) to evaluate the temperature dependence of the theoretical sensing response and Arrhenius-estimated recovery time.

Motivation, Novelty, and Significance

This study is driven by the urgency for innovative and diagnostic techniques that are non-intrusive and effective in early detection of lung cancer. Although the general concept of breath analysis is promising, the ability to translate this concept into clinical practice requires the development of sensing materials with high sensitivity and selectivity that are able to detect trace VOC biomarkers in complex exhaled breath matrices. The intrinsic chemical inertness and limited selectivity of carbon nanotubes make them appealing options for such sensors, but they require strategic

modification. The novelty of this work lies in examining the chirality-dependent response of Ag-functionalized SWCNT models toward two lung-cancer-associated VOCs using a consistent first-principles framework. In contrast to the earlier studies that considered only adsorptions with a single CNT configuration, we show that by combining the chiral dependence of the adsorption and electronic properties, different chirality-dependent adsorption and electronic responses toward benzene and styrene are obtained, with Ag-zigzag having a greater sensitivity to benzene and Ag-armchair for styrene. This anisotropy is being used as another design parameter when developing sensors, which has not been extensively studied for spintronics involving Ag-functionalized CNT. Additionally, the analysis of the sensing response and recovery time of the sensor as a function of the temperature over the range 300-500K gives practical guidelines for design of reversible gas sensors, which was a critical aspect missing from the literature. The value of this study is in providing a theoretical basis for the rational design of chirality-selective gas sensor for non-invasive lung cancer screening. The results showed that carbon nanotubes could be engineered to exhibit a specific degree of doping and thus specific response to a specific VOC, allowing the possibility to build an array of carbon nanotubes that could distinguish between multiple biomarkers by pattern recognition methods. The Arrhenius-type calculations predict short theoretical recovery times for some configurations at elevated temperatures, although these values depend on the assumed attempt frequency and adsorption energy and should not be interpreted as experimentally demonstrated recyclability. It contributes to the fundamental understanding of chirality-dependent sensing mechanisms and theoretical framework for next generation gas sensors for future investigation of breath-based sensing approaches.

2. Computational Details

2.1 DFT Calculations

All the calculations were done with the density functional theory (DFT) code available within the SIESTA package [37]. A generalized gradient approximation (GGA) using the exchange–correlation functional of Perdew–Burke–Ernzerhof (PBE) was used [38]. Norm-conserving pseudopotentials and a double-zeta polarized (DZP) basis set was used to describe the valence electron configurations, and was utilized for all atoms [39]. Brillouin zone sampling was performed with a plane-wave cutoff of 200 Ry, and a Monkhorst–Pack k-point mesh of 1×1×20.

2.2 Structural Models

Single-walled carbon nanotubes (SWCNTs) with explicitly defined chiral indices were constructed in Materials Studio. The armchair and zigzag nanotubes were modeled as (4,4) and (8,0) SWCNTs, respectively. The (4,4) armchair SWCNT consisted of 64 carbon atoms with a diameter of approximately 5.42 Å and a periodic length of 9.84 Å, whereas the (8,0) zigzag SWCNT consisted of 64 carbon atoms with a diameter of approximately 6.26 Å and a periodic length of 17.04 Å. The nanotube axes were oriented along the corresponding periodic directions. A single Ag atom was initially positioned approximately 3.0 Å from the nanotube sidewall and the complete structures were subsequently geometry optimized.

2.3 Adsorption Energy Calculation

The adsorption energy (Eb) was calculated using the following equation:

$$E_b = E_{gas\text{-}SWCNTs} - E_{SWCNTs} - E_{gas}$$

Here, $E_{gas\text{-}SWCNTs}$ represents the energy of the whole system containing the gas molecule and the Ag doped CNT, E_{SWCNTs} the energy of the free Ag doped CNT and E_{gas} the energy of the free gas molecule. Endothermic adsorption needs energy to be added to the exterior and $Eb > 0$, whereas exothermic adsorption involves stable complex formation and $Eb < 0$.

2.4 Sensing Response and Recovery Time

The sensing response was estimated from the change in electrical conductivity associated with the variation of the electronic band gap upon VOC adsorption. The electrical conductivity was approximated according to

$$\sigma \propto exp\left(-\frac{E_g}{2K_BT}\right)$$

where σ is the electrical conductivity, Eg is the electronic band gap, kB is the Boltzmann constant, and T is the absolute temperature. Accordingly, the dimensionless sensing response was evaluated as

$$S = \left|\frac{\sigma_{ads}}{\sigma_{pristine}} - 1\right| = exp\left(\frac{|\Delta E_g|}{2K_BT}\right) - 1$$

where,

$$\Delta E_g = E_g^{ads} - E_g^{pristine}$$

The recovery time was estimated using the conventional Arrhenius-type expression

$$\tau = \upsilon_0^{-1} exp\left(-\frac{E_{ads}}{K_B T}\right)$$

where Eads is the adsorption energy, kB is the Boltzmann constant, T is the absolute temperature, and ν_0 is the attempt frequency. For exothermic adsorption energies, the expression is equivalent to $\tau = \nu_0^{-1} \exp\left(\frac{|E_{ads}|}{K_B T}\right)$. The attempt frequencies used for the light-assisted estimates must be stated consistently with the corresponding illumination conditions.

The sensing-response values in Table 3 were obtained from the band-gap difference between the corresponding Ag-functionalized CNT and VOC-adsorbed configuration at each temperature using Equation of sensing response. The band-gap values used in this calculation are listed in Table 2.

3. Results and Discussion

3.1 Geometrical Analysis

The optimized geometries of benzene and styrene adsorbed on Ag-SWCNT (armchair) and (zigzag) are presented in Fig. 1 and Fig. 2, respectively. In the armchair structure, two carbon atoms from the benzene ring are joined to the Ag atom at 2.308 Å and at 2.463 Å, and two carbon atoms of the styrene ring are joined at 2.287 Å and 2.408 Å. At the zigzag geometry, distances of 2.340 Å and 2.377 Å between the benzene and the Ag atoms, respectively, find the styrene–Ag distances as 2.301 Å and 2.346 Å. The optimized Ag–C distances indicate close contact between the aromatic molecules and the Ag-functionalized CNT surface. Together with the calculated adsorption energies and PDOS features, these geometrical characteristics provide evidence for appreciable adsorbate–surface interaction in the exothermically adsorbed configurations. The total number atoms in the C_6H_6-Ag-SWCNT complexes is 77 (with 3 atomic species: C, H, Ag) while the C_8H_8-Ag-SWCNT complexes have 81 atoms. Changes in bond lengths upon adsorption are observed, which is consistent with that reported for metal doped CNT system. Pd–C bond distances

were found to be about 2.1–2.4 Å by yoosefian et al. for styrene on Pd-doped SWCNTs [29] which are similar to our calculated distances. Likewise, the distances of the metal–carbon bond (Ni–C) range between 2.1–2.5 Å in Ni-doped SWCNTs and aromatic VOCs [13]. The subtle bond lengths differences between armchair and zigzag configuration (see for example 2.308 Å vs. 2.340 Å for benzene) are merely a reflection of the different local curvature and electronic structure of the two chiralities. Ag–C bond distances are very close to the sum of the covalent radii for Ag (1.45Å) and C (0.77Å) indicating that the calculated Ag–C distances indicate close interaction between Ag and the CNT framework; however, a quantitative bonding analysis would be required to determine the detailed nature of the Ag–C interaction.

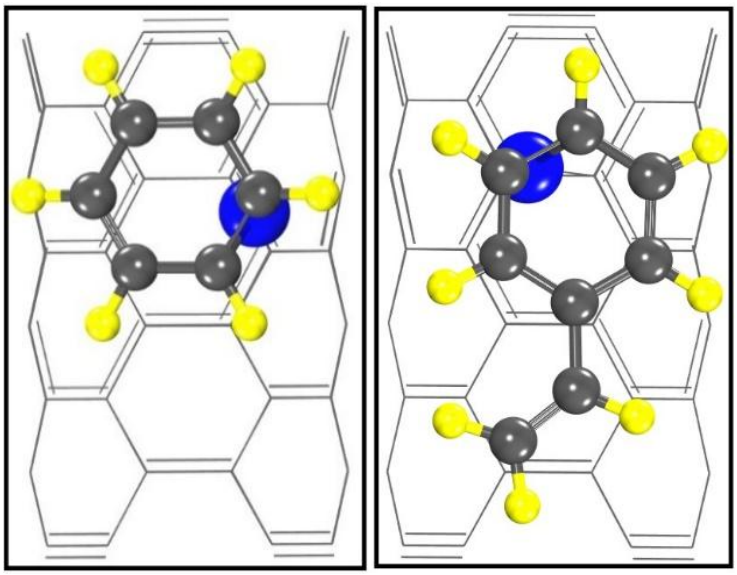


Figure 1. Optimized geometry of (a) C_6H_6-Ag-CNT armchair and (b) C_8H_8-Ag-CNT armchair.

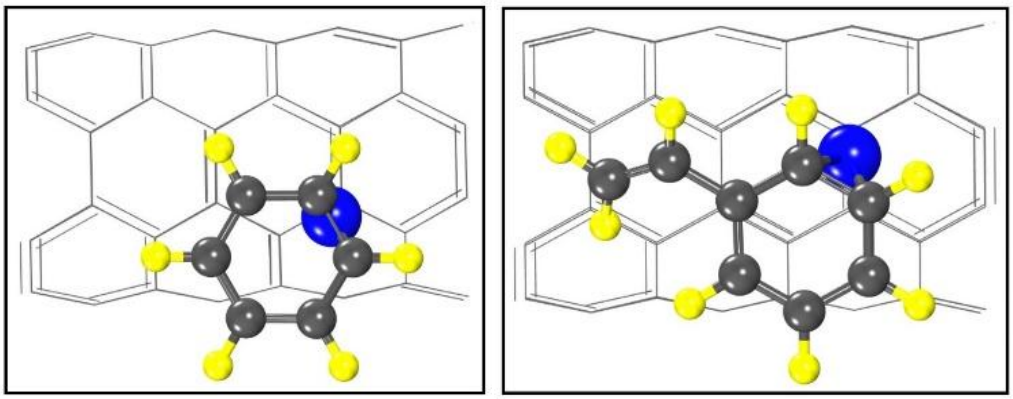


Figure 2. Optimized geometry of (a) C_6H_6-Ag-CNT zigzag and (b) C_8H_8-Ag-CNT zigzag.

3.2 Adsorption Energy Analysis

The adsorption energies for benzene and styrene with both Ag-CNT configurations are displayed in Table 1. The results reveal that the adsorption of benzene molecule is endothermic for Ag-zigzag with the value of Eb as 0.71 eV, while Ag-armchair is exothermic with Eb of −0.32 eV. For styrene, the exothermic adsorption character is present for both CNT configurations with exothermic ΔE for Ag-armchair (−0.94 eV) being more pronounced than for Ag-zigzag (−0.49 eV).

Table 1. Adsorption energies (Eb) of benzene and styrene on Ag-doped armchair and zigzag CNTs.

System	Eb (eV)	Adsorption Type
C_6H_6-Ag CNT armchair	−0.32	Exothermic
C_8H_8-Ag CNT armchair	−0.94	Exothermic
C_6H_6-Ag CNT zigzag	0.71	Endothermic
C_8H_8-Ag CNT zigzag	−0.49	Exothermic

The calculated band-gap-based sensing response is larger for the benzene/Ag-zigzag configuration; however, because its adsorption energy is positive, this configuration should be interpreted cautiously and does not by itself establish a thermodynamically favorable sensing state.

The anisotropic behavior is related to the different electronic structure of the two chiralities: it affects the orbital overlap between the dopant (Ag) and the adsorbent molecules. For comparison, Yoosefian et al. reported an adsorption energy of −1.27 eV for styrene on Pd-doped SWCNTs, whereas the present Ag-armchair system gives −0.94 eV. Thus, the two values indicate comparable but not identical adsorption strengths [29]. The apparent similarity with respect to the DOS affinity of various aromatic VOCs on the different metal-doped CNTs imply that the interaction between the π bond and the metal ions is the key, more important, factor than the nature of the transition metal to the DOS affinity. Aasi et al. reported the range of adsorption energies from −0.5 to −1.2 eV for the adsorption of toluene molecules (a methyl substituted benzene) on the Pt-decorated CNTs [30] the calculated adsorption energy of benzene on Ag-zigzag is positive (+0.71 eV), indicating that the optimized adsorbed configuration is energetically unfavorable relative to the separated Ag-zigzag CNT and benzene molecule under the adopted adsorption-energy convention. Therefore, this configuration should not be interpreted as a thermodynamically favorable adsorption state solely on the basis of the optimized geometry. Nevertheless, the calculated electronic-structure modification associated with this configuration can be discussed as a theoretical response of the optimized complex, with appropriate caution. Because the calculated adsorption energy is positive, the benzene/Ag-zigzag configuration is not energetically favorable relative to the separated components under the present definition of Eb. Consequently, its suitability as a reversible sensing configuration should not be inferred from the adsorption energy alone.

3.3 Energy Band Structure

The band structures of pristine and Ag-doped armchair and zigzag SWCNTs both before and after the adsorption of VOCs are shown in Figure 3 and Figure 4, respectively. Bandgaps were calculated and compared to other available values; the results are summarized in Table 2.

Table 2. Bandgap (Eg) and Fermi energy (EF) values for all systems, compared with available literature data.

Material	Eg (eV)	EF (eV)	Reference
Armchair	**0.05**	**−3.95**	**0.042 (DFT), 0.08 (Exp) [40]**

Material	Eg (eV)	EF (eV)	Reference
Zigzag	0.005	−3.96	0.041 (DFT) [40]
Ag-Armchair	0.02	−3.67	—
Ag-Zigzag	0.02	−3.91	—
C_6H_6-Ag Armchair	0.06	−3.48	—
C_6H_6-Ag Zigzag	0.11	−3.27	—
C_8H_8-Ag Armchair	0.06	−3.49	—
C_8H_8-Ag Zigzag	0.05	−3.51	—

The calculated band gaps of the pristine CNT models are reported for the specific chiralities employed in this work. Direct comparison with literature values must be made only for nanotubes having the same chiral indices and comparable computational methodology, because CNT band gaps depend strongly on chirality and diameter. Therefore, the present PBE results are used primarily as a consistent reference for evaluating the changes induced by Ag functionalization and VOC adsorption. Also, the zigzag CNT bandgap (0.005 eV) is in accord with the near-metallic nature of this structure. The armchair CNT is narrowed down from 0.05eV to 0.02eV and the zigzag CNT is broadened from 0.005eV to 0.02eV when it is Ag doped. The present bandgap modification due to metal doping correlates well with the results reported by Yuksel and coworkers who reported that SWCNTs doped with Pd, Ag and Rh show modifications of their HOMO–LUMO gap [33]. Following VOC adsorption, the band gaps of the complexes change as follows: in the armchair configuration, adsorption of benzene and styrene produces a calculated band gap of 0.06 eV, whereas the zigzag configuration exhibits band gaps of 0.11 eV for benzene adsorption and 0.05 eV for styrene adsorption. These changes indicate molecule- and chirality-dependent modification of the electronic structure. The larger band gap calculated for benzene-Ag-zigzag compared with styrene-Ag-zigzag is consistent with the different adsorption characteristics of the two configurations. The shifts in Fermi energy following Ag functionalization and VOC adsorption

indicate changes in the electronic structure of the combined systems; however, quantitative charge-transfer analysis would be required to establish the magnitude and direction of electron redistribution. The greater band gap (0.11 eV) of benzene-Ag-zigzag than that of styrene-Ag-zigzag (0.05 eV) has been observed, which is consistent with the positive value of adsorption energy for benzene on Ag-zigzag. The shift in Fermi energy upon Ag functionalization and VOC adsorption indicates a modification of the electronic structure of the combined systems. However, the magnitude and direction of electron redistribution cannot be established quantitatively from the band structures alone and would require a dedicated charge-transfer analysis.

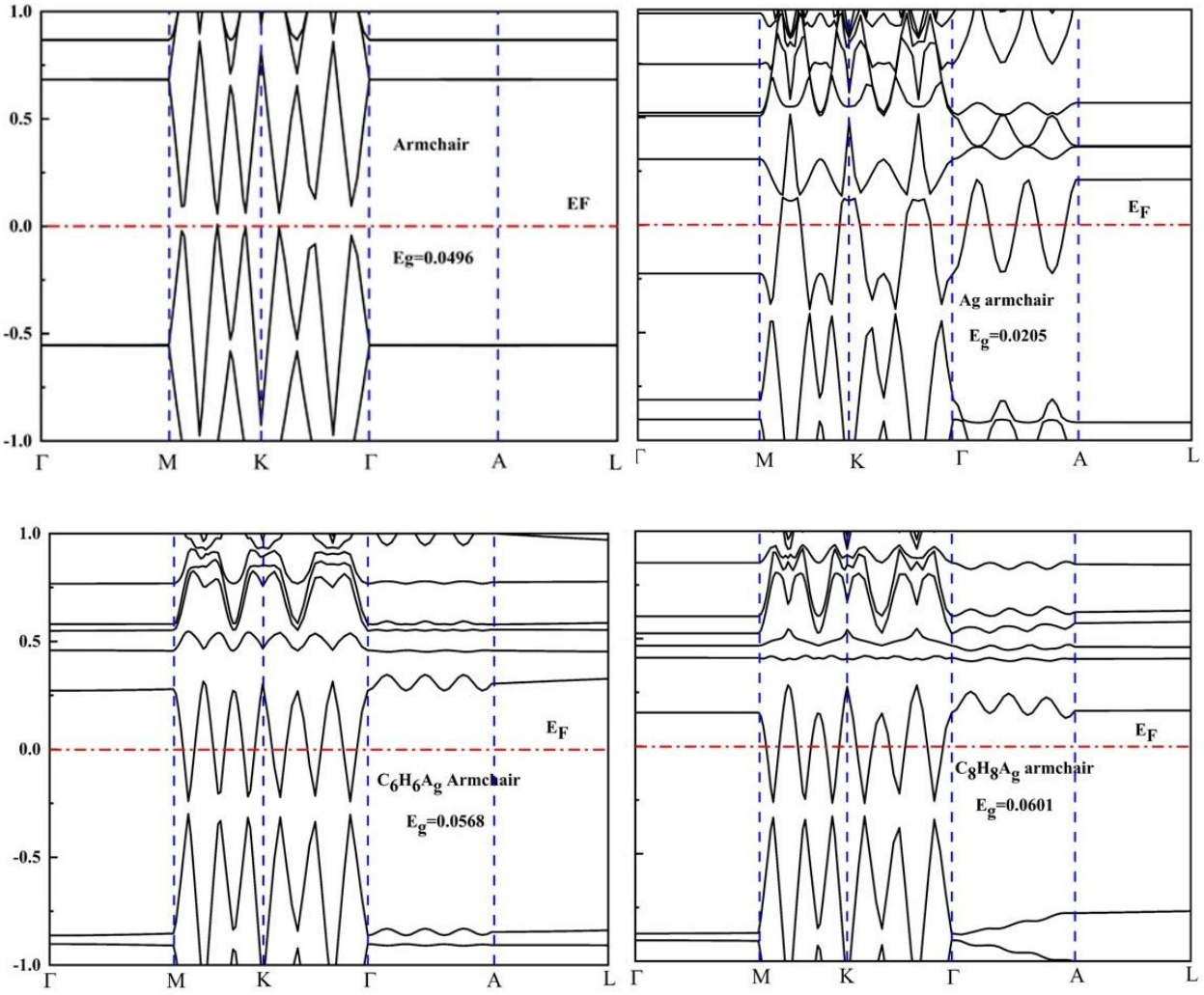


Figure 3. Band structure of (a) armchair, (b) Ag-armchair, (c) benzene-Ag-armchair, and (d) styrene-Ag-armchair.

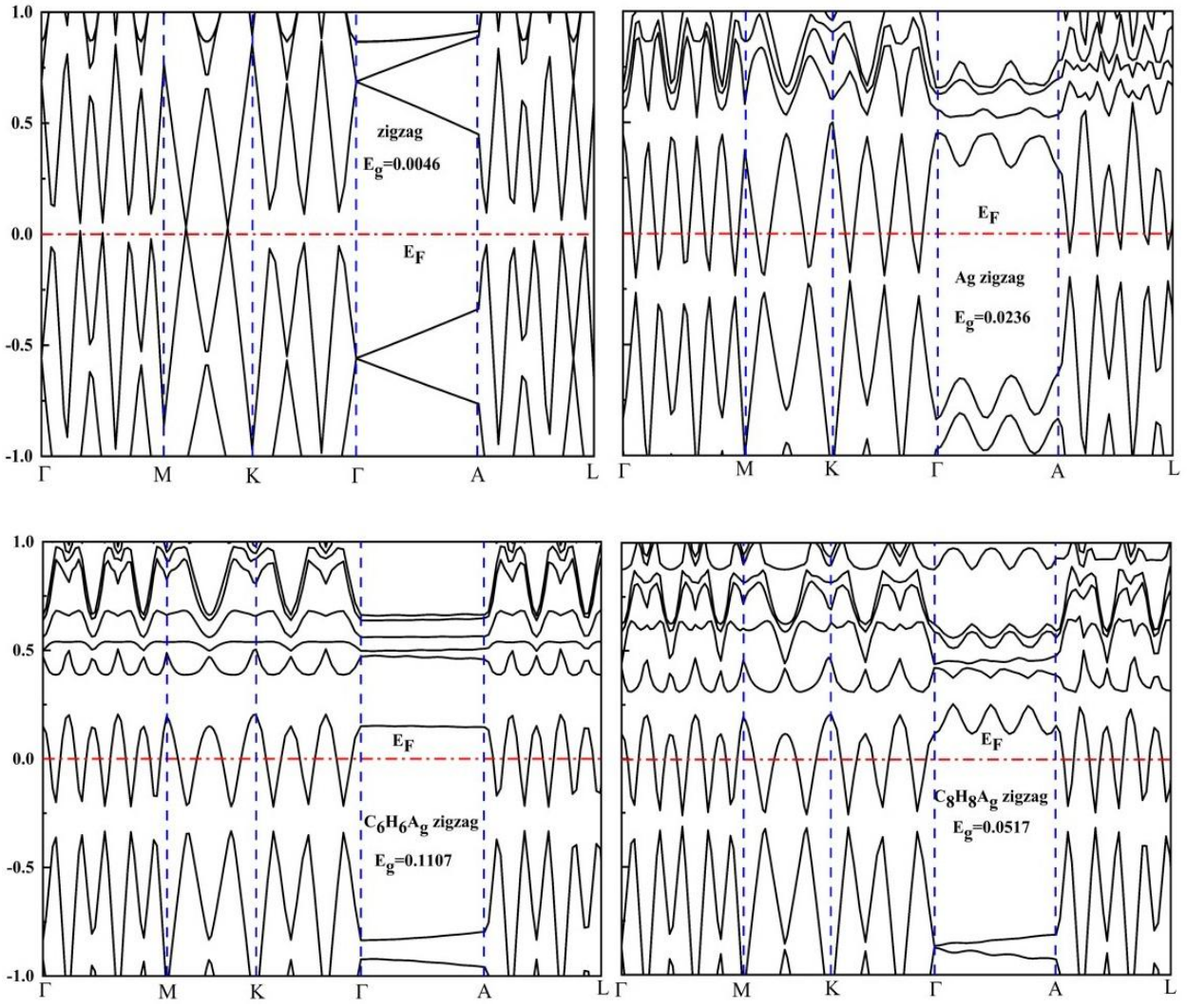
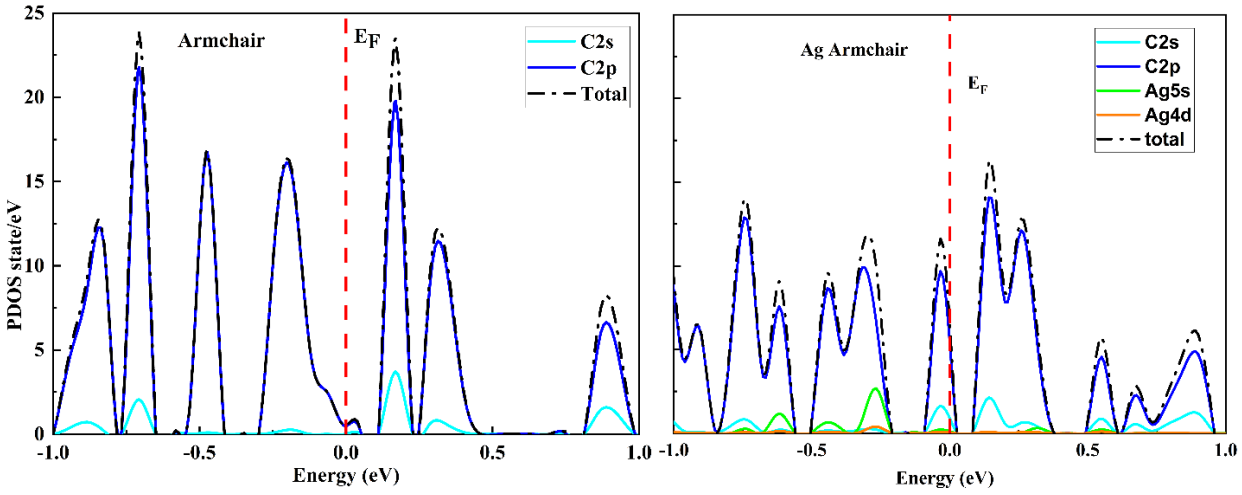


Figure 4. Band structure of (a) zigzag, (b) Ag-zigzag, (c) benzene-Ag-zigzag, and (d) styrene-Ag-zigzag.

3.4 Projected Density of States (PDOS)

All the systems are shown to have the same PDOS in Figures 5 and 6, which helps provide insight into the orbital contributions associated with the electronic structure. In the case of CNTs that have not been doped, the conduction and valence bands consist of C2s and C2p orbitals. Ag functionalization generates Ag 5s and Ag 4d states appear near the Fermi-level region, introducing additional electronic states that modify the electronic structure of the CNT and may contribute to the calculated sensing response. This observation is confirmed by Gracia-Espino et al. who found

a presence of Ag 4d and 5s states in the vicinity of the Fermi level upon silver decoration of CNTs, the enhanced density of states as well as the difference in electrical resistance [41]. The H1s orbitals contribute to the valence band upon the adsorption of VOCs, representing the hybridization between the VOC molecules and the surface of CNT, which supports this. The appearance and energy overlap of H 1s states with the electronic states of the adsorbate–CNT complex is consistent with electronic hybridization between the VOC molecule and the Ag-functionalized CNT. The PDOS analysis additionally indicates that The PDOS indicates appreciable Ag 4d contributions in the energy region associated with the adsorbate-induced electronic states, suggesting hybridization between Ag-derived states and the π states of the aromatic molecules. This orbital overlap provides a possible electronic interpretation of the calculated adsorption behavior, as they strongly hybridize with π states of aromatic rings. The strong adsorption of the VOCs on metal-doped CNTs follows the dominant d-π hybridization model as proposed by Aasi et al., for platinum group metal-decorated SWCNTs [30]. In the PDOS of the benzene-Ag-zigzag system, the contribution of the H1s states in the valence band is indeed smaller than is the case for the styrene-Ag-armchair systems, which is consistent with the weaker calculated interaction of benzene with Ag-zigzag based on its positive adsorption energy



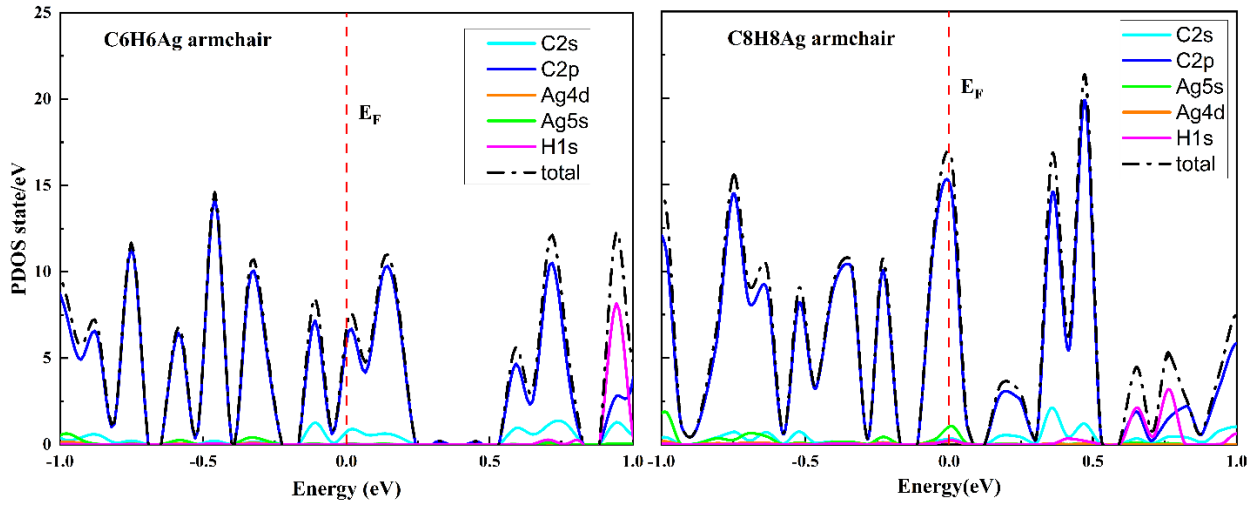


Figure 5. PDOS of (a) armchair, (b) Ag-armchair, (c) benzene-Ag-armchair, and (d) styrene-Ag-armchair.

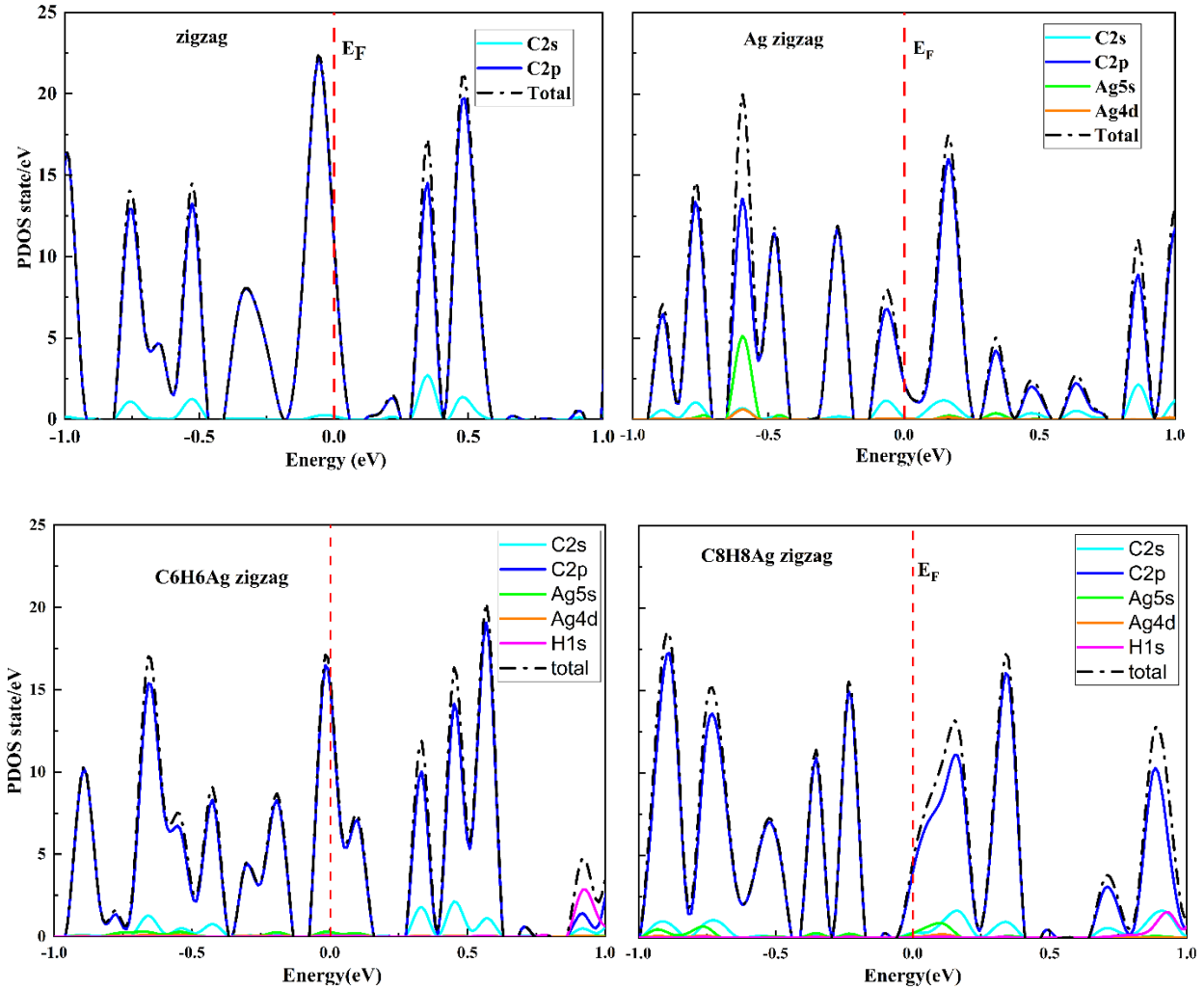


Figure 6. PDOS of (a) zigzag, (b) Ag-zigzag, (c) benzene-Ag-zigzag, and (d) styrene-Ag-zigzag.

3.5 Optical Properties

3.5.1 Absorption Coefficient

The absorption coefficients of all systems are given in Figure 7. Pristine armchair CNT has a higher absorption than pristine zigzag CNT. When doped with Ag atom, the absorption coefficient of both the configurations improves, and becomes close to one another. The benzene adsorption result indicates that the absorption is higher for the Ag-armchair as compared to the Ag-zigzag, similarly it shows the same trend for styrene. The modified optical absorption can be associated with changes in the electronic states and allowed interband transitions introduced by Ag functionalization and VOC adsorption. Although changes in the calculated band gap may contribute to the spectral response, the absorption intensity is also governed by the available electronic states and transition matrix elements. When the energy is greater than 4.5 eV, the absorption coefficient drops, because the energy is not absorbed by the medium. The result is in accordance with that of Ouyang et al., which has found that defect induced by doping with metals generates mid-gap state and increases the density of state near the Fermi level, which lead to enhanced optical absorption of metal doped CNTs [42]. It was observed that Ag-armchair shows the maximum absorption coefficient at the resonance peaks, followed by Ag-zigzag among all the compositions indicated that the calculated optical absorption of the Ag-armchair configuration is higher than that of Ag-zigzag over substantial portions of the investigated energy range, suggesting that chirality may influence the optical response of Ag-functionalized CNTs.

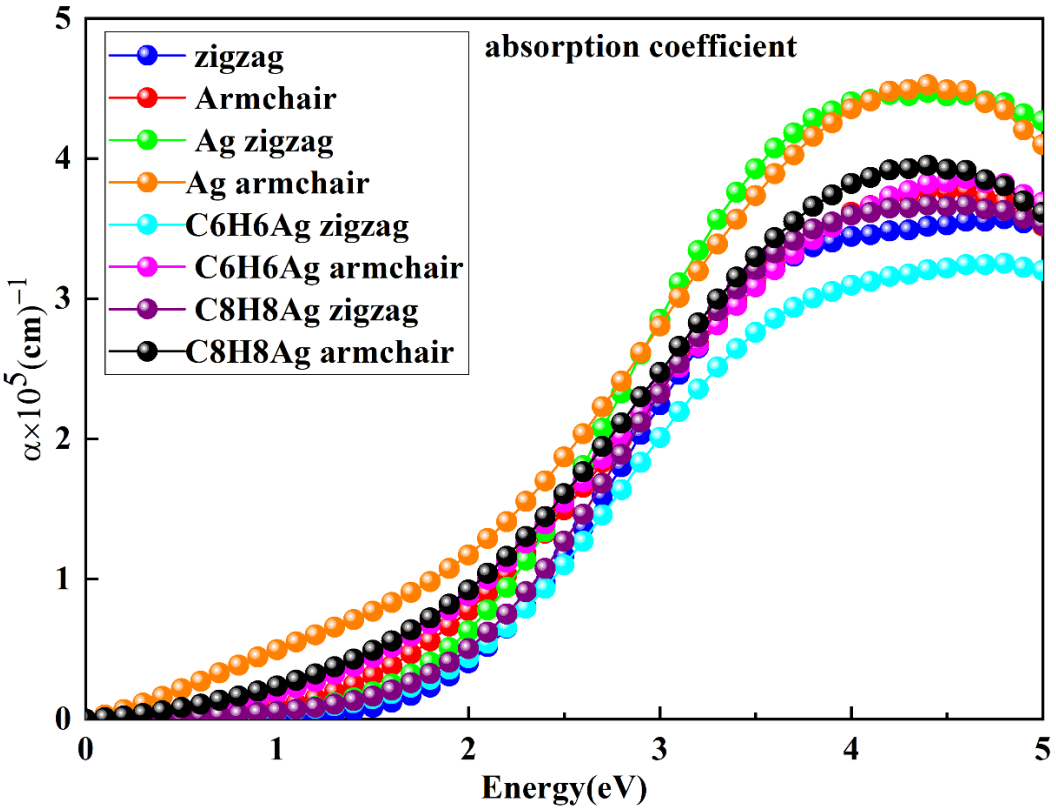


Figure 7. Absorption coefficient of pristine CNTs, Ag-functionalized CNTs, and VOC-adsorbed complexes.

3.5.2 Optical Conductivity

These are the optical conductivity σ of all systems presented in Figure 8. Pristine CNTs have low value of optical conductivity and enhances significantly after Ag functionalization. The calculated optical conductivity of all systems is presented in Figure 8. The pristine CNTs exhibit lower optical conductivity over much of the investigated energy range, whereas Ag functionalization produces a substantial modification of the optical response. Among the Ag-functionalized systems, Ag-zigzag exhibits the highest optical conductivity near the main maximum, while VOC adsorption further modifies the spectral response depending on both the molecule and CNT chirality. The maximum optical conductivity is found at ~3.5 eV, which also agrees with the absorption coefficient data. The enhancement and redistribution of the optical conductivity following Ag functionalization can be associated with the appearance of Ag-derived electronic states, particularly Ag 5s and 4d contributions, near the Fermi-level region. The PDOS results indicate hybridization between Ag-derived states and the CNT electronic states; however, a quantitative

charge-transfer analysis would be required to establish the magnitude and direction of electron transfer. This trend is qualitatively consistent with experimental studies reporting modified gas-sensing behavior following Ag nanocrystal decoration of CNT-based sensors (Cui et al.), which showed that the conductivity of the CNT-based gas sensor is greatly increased at room temperature when decorated with Ag nanocrystals [31]. The relationship between the absorption coefficient and the optical conductivity is to be expected since both are governed by the joint density of states and by the elements of the transition matrix. Ag-zigzag has the highest optical conductivity of all of the compositions while C_6H_6-Ag zigzag has the lowest optical conductivity value at 3.5 eV.

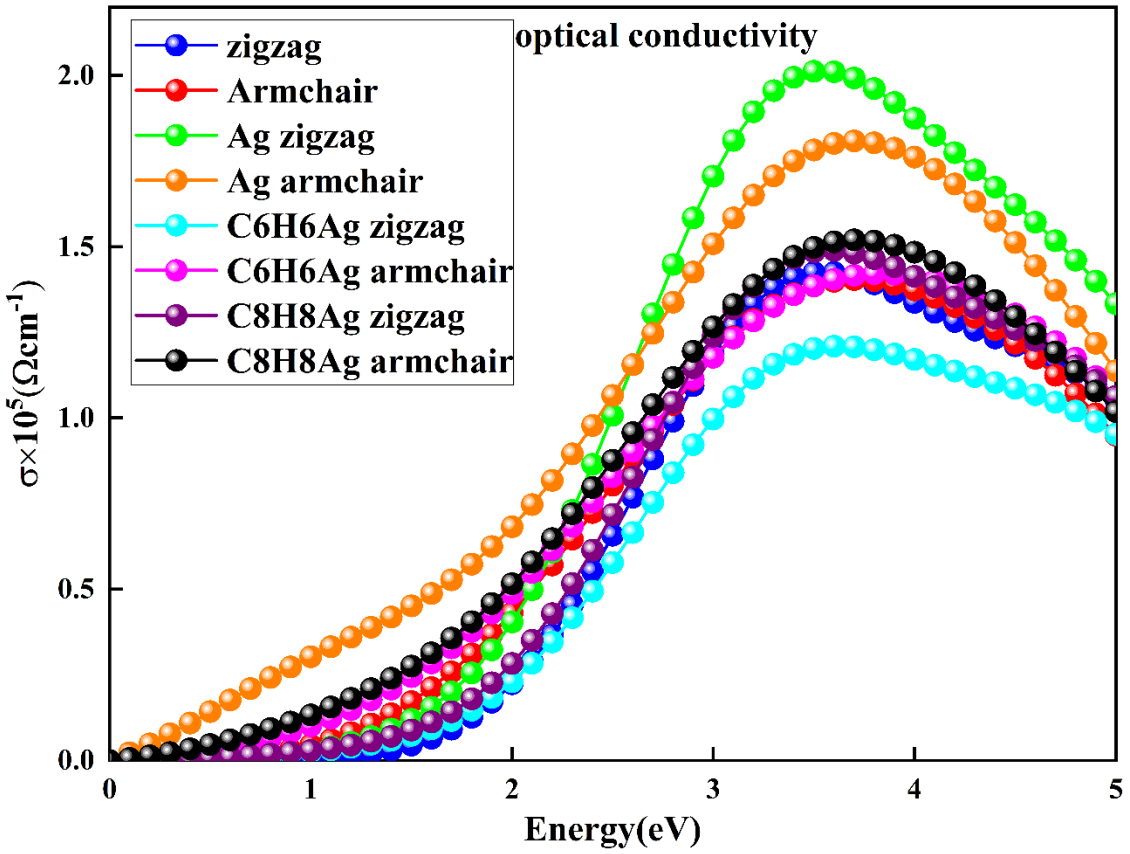


Figure 8. Optical conductivity of pristine CNTs, Ag-functionalized CNTs, and VOC-adsorbed complexes.

3.6 Sensing Response and Recovery Time

The sensing response of Ag-armchair and Ag-zigzag to the target gases benzene and styrene has been calculated at different temperatures from 300 K to 500 K and is presented in Table 3. The

Ag-zigzag has the highest sensing response on benzene (4.39 at 300 K), and Ag-armchair has the highest sensing response for styrene (1.15 at 300 K). All systems show a decreasing sensing response with increase of temperature because of increased thermal agitation of the charge carriers that decreases the relative change of conductivity upon gas adsorption. The values of the sensing response reported here, are either similar or higher than those reported for other metal doped CNT system. For example, Ni-doped SWCNTs were reported by Wan et al. to sense the response to benzene and styrene under room temperature [13]. The sensing response to benzene of our Ag-zigzag system at 300 K is 4.39, indicating favorable performance in sensing. The sensing response of Ag-Zigzag towards benzene (4.39 at 300K) is also greater than the sensing response of the Rh-doped CNTs towards benzene (3.94 at 300K) reported by Wan et al. [27].

Table 3. Sensing response of different VOCs on Ag-armchair and Ag-zigzag at various temperatures.

Temperature (K)	C_6H_6-Ag Armchair	C_8H_8-Ag Armchair	C_6H_6-Ag Zigzag	C_8H_8-Ag Zigzag
300	**1.02**	**1.15**	**4.39**	**0.72**
350	**0.82**	**0.92**	**3.24**	**0.59**
400	**0.69**	**0.77**	**2.54**	**0.50**
450	**0.59**	**0.66**	**2.07**	**0.44**
500	**0.52**	**0.58**	**1.75**	**0.38**

***(Table Note:** The C_6H_6–Ag-zigzag value represents the calculated electronic response of the optimized complex; because its adsorption energy is positive (+0.71 eV), this configuration is not considered a thermodynamically favorable adsorption state.)*

The estimated recovery times are summarized in Table 4 for the exothermically adsorbed configurations. The recovery time decreases exponentially with increasing temperature because thermal energy facilitates desorption. For a given adsorption configuration, the estimated recovery time under the UV attempt-frequency assumption is four orders of magnitude smaller than that obtained under the visible-light attempt-frequency assumption because 10^{16} s^{-1} is four orders of magnitude larger than 10^{12} s^{-1}. The C_6H_6–Ag-armchair configuration exhibits a short-estimated recovery time, reaching approximately 1.68×10^{-9} s at 500 K under the visible-light attempt-frequency assumption. In contrast, the C_8H_8–Ag-armchair configuration has a substantially longer estimated recovery time because of its stronger adsorption energy of −0.94 eV. The C_8H_8–Ag-zigzag configuration exhibits shorter estimated recovery times because its adsorption energy is −0.49 eV. A recovery time is not assigned to the C_6H_6–Ag-zigzag configuration because its calculated adsorption energy is positive (+0.71 eV), indicating an energetically unfavorable adsorption configuration under the adopted convention. These values should be regarded as Arrhenius-type theoretical estimates rather than experimentally measured recovery times [6].

Table 4. Estimated recovery times of VOCs adsorbed on Ag-functionalized SWCNTs under visible and UV conditions.

VOC–CNT system	Eads (eV)	Vis, 300 K	Vis, 350 K	Vis, 400 K	Vis, 450 K	Vis, 500 K	UV, 300 K	UV, 350 K	UV, 400 K	UV, 450 K	UV, 500 K
C_6H_6–Ag-armchair	−0.32	2.38×10^{-7}	4.05×10^{-8}	1.08×10^{-8}	3.84×10^{-9}	1.68×10^{-9}	2.38×10^{-11}	4.05×10^{-12}	1.08×10^{-12}	3.84×10^{-13}	1.68×10^{-13}
C_8H_8–Ag-armchair	−0.94	6.19×10^{3}	3.43×10^{1}	6.97×10^{-1}	3.37×10^{-2}	2.98×10^{-3}	6.19×10^{-1}	3.43×10^{-3}	6.97×10^{-5}	3.37×10^{-6}	2.98×10^{-7}
C_6H_6–Ag-	+0.71	N/A	N/A	N/A	N/A	N/A	N/A	N/A	N/A	N/A	N/A

zigzag											
C_8H_8–Ag-zigzag	**−0.49**	**1.71×10^{-4}**	**1.14×10^{-5}**	**1.49×10^{-6}**	**3.07×10^{-7}**	**8.69×10^{-8}**	**1.71×10^{-8}**	**1.14×10^{-9}**	**1.49×10^{-10}**	**3.07×10^{-11}**	**8.69×10^{-12}**

Units: seconds.

***(Table note:** Recovery times were estimated using $\tau = \nu_0^{-1} \exp(-E_{ads}/kBT)$, with $\nu_0 = 10^{12}\ s^{-1}$ for the visible-light condition and $\nu_0 = 10^{16}\ s^{-1}$ for the UV condition. Recovery-time estimates are reported only for exothermic adsorption configurations. The positive adsorption energy calculated for C_6H_6–Ag-zigzag indicates an energetically unfavorable adsorption configuration under the adopted convention; therefore, a physically meaningful recovery-time estimate is not assigned.)*

The sensing property of Ag-functionalized CNTs is comparable to the other CNT sensors with reported in the literature. As reported by Wan et al. [26], adsorption energy of both benzene and styrene on the Pt loaded CNTs has followed similar trend as our results. Aasi et al. proved that the decoration of transition metal promotes the adsorption of VOCs on CNTs via charge transfer interactions [30]. The selectivity of Rh-doped CNTs for benzene and aniline with high changes in conductivity was noticed after CO_2 adsorptions whereas it remained unaffected to CO_2 [27]. The two investigated CNT chiralities exhibit different theoretical responses toward benzene and styrene, indicating chirality-dependent response characteristics. However, a rigorous assessment of chemical selectivity would require calculations involving additional competing breath constituents and interfering gases. The different responses of the armchair and zigzag configurations suggest that CNT chirality may provide an additional design parameter for distinguishing VOC-induced electronic responses. However, validation against additional competing VOCs would be required to establish chemical selectivity. This feature might be beneficial in situations of the sensor pairs, such as zigzag and armchair providing orthogonal responses, and allowing the pattern recognition approach to identify multiple biomarkers.

3.7 Limitations and Scope of the Present Study

Several limitations of the present theoretical investigation should be noted. First, the calculations employ the PBE generalized-gradient approximation, which can underestimate electronic band gaps; therefore, the absolute band-gap values should be interpreted primarily in terms of relative changes induced by Ag functionalization and VOC adsorption. Second, the models represent idealized isolated CNT/VOC configurations containing a single adsorbed molecule and do not explicitly account for competitive adsorption among multiple breath constituents, humidity, oxygen, carbon dioxide, nitrogen, or other environmental interferents. Third, the theoretical sensing response is derived from band-gap-dependent conductivity relations rather than from an explicit device-level transport calculation, such as nonequilibrium Green's-function simulations or experimental conductance measurements. Fourth, the recovery times are Arrhenius-type estimates that depend on the assumed attempt frequency and adsorption energy and therefore should not be interpreted as experimentally measured response or recovery times. Fifth, no concentration-dependent detection-limit analysis, sensor noise analysis, or clinical breath-sample validation was performed. Consequently, the present results should be regarded as a first-principles screening and mechanistic study that identifies chirality-dependent electronic and adsorption trends rather than as a direct demonstration of clinical lung-cancer diagnosis. Experimental measurements and device-level simulations involving realistic breath matrices will be required to establish the practical sensing performance of Ag-functionalized CNTs.

4. Conclusions

In this work, density functional theory calculations were employed to investigate the chirality-dependent interaction of benzene and styrene with Ag-functionalized single-walled carbon nanotubes. The optimized structures, adsorption energies, electronic band structures, projected density of states, optical properties, theoretical sensing responses, and Arrhenius-estimated recovery times were systematically analyzed for armchair and zigzag configurations. The calculated adsorption energies reveal distinct molecule- and chirality-dependent interactions. Styrene exhibits exothermic adsorption on both Ag-functionalized configurations, with the strongest calculated interaction obtained for the Ag-armchair configuration (−0.94 eV). In contrast, benzene exhibits an exothermic interaction with Ag-armchair (−0.32 eV) but a positive adsorption energy (+0.71 eV) for the optimized Ag-zigzag configuration, indicating that the latter is energetically unfavorable relative to the separated components under the adopted convention.

These results demonstrate that CNT chirality can substantially influence the calculated interaction of aromatic VOCs with Ag-functionalized CNTs. Electronic-structure calculations show that Ag functionalization introduces Ag-derived electronic states and modifies the band gaps of the CNTs. VOC adsorption produces additional changes in the band structures and PDOS, indicating molecule-dependent modification of the electronic structure. The calculated optical spectra likewise exhibit chirality- and molecule-dependent changes in absorption coefficient and optical conductivity. The theoretical sensing response derived from the band-gap-dependent conductivity relation decreases with increasing temperature over the investigated 300–500 K range. Arrhenius-type recovery-time estimates also decrease with increasing temperature, although the absolute values depend on the assumed attempt frequency and adsorption energy and therefore should not be interpreted as experimentally measured recovery times.

Overall, the calculations demonstrate that Ag functionalization and CNT chirality can modify the predicted interaction and electronic response toward benzene and styrene. The results therefore provide a theoretical basis for further investigation of chirality-dependent CNT sensing of lung-cancer-associated VOCs. However, experimental sensor fabrication, concentration-dependent measurements, interference studies, realistic breath-matrix simulations, and clinical validation are required before conclusions regarding practical lung-cancer screening or diagnosis can be established.

Credit authorship contribution statement

Muhammad Yaseen, Shehroz Abdullah, Iqra Abdullah: Conceptualization, methodology, software, Validation, investigation, visualization, writing and original draft preparation.

Suhrab Khan, Faizan Ahmad Khan, Waqar Ahmad, Arslan Ahmad: Formal analysis

Dr. Muhammad Asif, Anila Asif: Supervision, validation, writing, review and editing.

Funding: This research received no specific grant from any funding agency in the public, commercial, or not-for-profit sectors.

Acknowledgments

The authors thank the Materials Modeling Lab, Department of Physics, Islamia College Peshawar Pakistan, and COMSATS University Islamabad, Lahore Campus, Pakistan, and Department of Physics University of Peshawar, Pakistan for computational support.

Declaration of competing interest

The authors declare that they have no known competing financial interests or personal relationships that could have appeared to influence the work reported in this paper.

Data availability

All data generated and analyzed during this study are presented in the manuscript. Additional computational data supporting the findings of this study are available from the corresponding author upon reasonable request.

References

1. Bray, F., Ferlay, J., Soerjomataram, I., Siegel, R. L., Torre, L. A., & Jemal, A. (2018). Global cancer statistics 2018: GLOBOCAN estimates of incidence and mortality worldwide for 36 cancers in 185 countries. *CA: A Cancer Journal for Clinicians*, 68(6), 394–424.

2. Sung, H., Ferlay, J., Siegel, R. L., Laversanne, M., Soerjomataram, I., Jemal, A., & Bray, F. (2021). Global cancer statistics 2020: GLOBOCAN estimates of incidence and mortality worldwide for 36 cancers in 185 countries. *CA: A Cancer Journal for Clinicians*, 71(3), 209–249.

3. Siegel, R. L., Miller, K. D., Fuchs, H. E., & Jemal, A. (2021). Cancer statistics, 2021. *CA: A Cancer Journal for Clinicians*, 71(1), 7–33.

4. National Lung Screening Trial Research Team. (2011). Reduced lung-cancer mortality with low-dose computed tomographic screening. *New England Journal of Medicine*, 365(5), 395–409.

5. Saalberg, Y., & Wolff, M. (2016). VOC breath biomarkers in lung cancer. *Clinica Chimica Acta, 459*, 5–9.

6. Khare, K. P., Srivastava, R., & Srivastava, A. (2025). Pristine and Pd doped carbon nanotube as a lung cancer biomarker for CO_2 and Rn gas: A DFT analysis. *Asian Journal of Research in Chemistry*, 18(5), 331–336.

7. Phillips, M., Gleeson, K., Hughes, J. M., Greenberg, J., Cataneo, R. N., Baker, L., & McVay, W. P. (1999). Volatile organic compounds in breath as markers of lung cancer: A cross-sectional study. *The Lancet*, 353(9168), 1930–1933.

8. Hakim, M., Broza, Y. Y., Barash, O., Peled, N., Phillips, M., Amann, A., & Haick, H. (2012). Volatile organic compounds of lung cancer and possible biochemical pathways. *Chemical Reviews*, 112(11), 5949–5966.

9. Amann, A., Mochalski, P., Ruzsanyi, V., Broza, Y. Y., & Haick, H. (2014). Assessment of the exhalation kinetics of volatile cancer biomarkers based on their physicochemical properties. *Journal of Breath Research*, 8(1), 016003.

10. Jia, Z., Patra, A., Kutty, V. K. K., & Venkatesan, T. (2019). Critical review of volatile organic compound analysis in breath and in vitro cell culture for detection of lung cancer. *Metabolites*, 9(3), 52.

11. Mazzone, P. J. (2008). Analysis of volatile organic compounds in the exhaled breath for the diagnosis of lung cancer. *Journal of Thoracic Oncology*, 3(7), 774–780.

12. Einoch Amor, R., Nakhleh, M. K., Barash, O., & Haick, H. (2019). Breath analysis of cancer in the present and the future. *European Respiratory Review*, 28(152), 190002.

13. Wan, Q., Xu, Y., & Zhang, X. (2017). Adsorption properties of typical lung cancer breath gases on Ni-SWCNTs through density functional theory. *Journal of Sensors*, 2017, 7974545.

14. Wan, Q., Chen, X., & Gui, Y. (2020). First-principles insight into a Ru-doped SnS_2 monolayer as a promising biosensor for exhale gas analysis. *ACS Omega*, 5(15), 8919–8926.

15. Freddi, S., & Sangaletti, L. (2022). Trends in the development of electronic noses based on carbon nanotubes chemiresistors for breathomics. *Nanomaterials*, 12(17), 2992.

16. Phillips, M., Cataneo, R. N., Cummin, A. R. C., Gagliardi, A. J., Gleeson, K., Greenberg, J., ... & Schmitt, P. (2003). Detection of lung cancer with volatile markers in the breath. *Chest*, 123(6), 2115–2123.

17. Iijima, S. (1991). Helical microtubules of graphitic carbon. *Nature*, 354(6348), 56–58.

18. Baughman, R. H., Zakhidov, A. A., & De Heer, W. A. (2002). Carbon nanotubes—the route toward applications. *Science*, 297(5582), 787–792.

19. De Volder, M. F., Tawfick, S. H., Baughman, R. H., & Hart, A. J. (2013). Carbon nanotubes: Present and future commercial applications. *Science*, 339(6119), 535–539.

20. Kong, J., Franklin, N. R., Zhou, C., Chapline, M. G., Peng, S., Cho, K., & Dai, H. (2000). Nanotube molecular wires as chemical sensors. *Science*, 287(5453), 622–625.

21. Collins, P. G., Bradley, K., Ishigami, M., & Zettl, A. (2000). Extreme oxygen sensitivity of electronic properties of carbon nanotubes. *Science*, 287(5459), 1801–1804.

22. Liu, P. (2005). Modifications of carbon nanotubes with polymers. *European Polymer Journal*, 41(11), 2693–2703.

23. Vardharajula, S., Ali, S. Z., Tiwari, P. M., Eroğlu, E., Vig, K., Dennis, V. A., & Singh, S. R. (2012). Functionalized carbon nanotubes: Biomedical applications. *International Journal of Nanomedicine*, 7, 5361–5374.

24. Zhang, T., Mubeen, S., Myung, N. V., & Deshusses, M. A. (2008). Recent progress in carbon nanotube-based gas sensors. *Nanotechnology*, 19(33), 332001.

25. Rahman, A. U., et al. (2025). A comparative DFT study on the effect of transition metals (Ru–Ag) on zero-dimensional fullerene and one-dimensional carbon nanotube. *International Journal of Computational Materials Science and Engineering*.

26. Wan, Q., Zhang, X., & Gui, Y. (2015). Theoretical study on Pt-doped carbon nanotubes used to detect typical exhaled gases of lung cancer. *Journal of Computational and Theoretical Nanoscience*, 12(10), 3412–3417.

27. Wan, Q., Xu, Y., Chen, X., & Xiao, H. (2018). Exhaled gas detection by a novel Rh-doped CNT biosensor for prediagnosis of lung cancer: A DFT study. *Molecular Physics*, 116(17), 2205–2212.

28. Wan, Q., Xu, Y., & Xiao, H. (2018). Exhaled gas detection by Ir-doped CNT for primary diagnosis of lung cancer. *AIP Advances*, 8(10), 105128.

29. Yoosefian, M., Ayoubi, E., & Atanase, L. I. (2022). Palladium-doped single-walled carbon nanotubes as a new adsorbent for detecting and trapping volatile organic compounds: A first principle study. *Nanomaterials*, 12(15), 2572.

30. Aasi, A., Aghaei, S. M., & Panchapakesan, B. (2020). A density functional theory study on the interaction of toluene with transition metal decorated carbon nanotubes: A promising platform for early detection of lung cancer from human breath. *Nanotechnology*, 31(41), 415707.

31. Cui, S., Pu, H., Mattson, E. C., Lu, G., Mao, S., Weinert, M., ... & Chen, J. (2012). Ag nanocrystal as a promoter for carbon nanotube-based room-temperature gas sensors. *Nanoscale*, 4(19), 5887–5894.

32. Chen, D., Cao, Z., & Yuan, Y. J. (2020). Investigation of formaldehyde adsorption on carbon nanotubes by density functional theory. Current Nanoscience, 16(5), 846–850.

33. Yuksel, N., Kose, A., & Fellah, M. F. (2022). Pd, Ag and Rh doped (8,0) single-walled carbon nanotubes (SWCNTs): A DFT study on furan adsorption and detection. Surface Science, 715, 121939.

34. Abdullah, S., Murtaza, G., Javed, A., Qayyum, B., & Asif, M. (2026). A comprehensive DFT study of two-dimensional semiconductors: Showcasing an analysis of the emerging 2D $InAg(PSe_3)_2$ monolayers for next-generation optoelectronic solicitations. *Chemical Physics*, 608, 113247.

35. Abdullah, S., Murtaza, G., Ali, A. B. M., Khaydarov, I., Elattar, S., Ahmad, Y., ... & Khan, M. I. (2026). First-principles investigation of optoelectronic and photocatalytic properties of Janus SnSSe monolayer. *Journal of Physics and Chemistry of Solids*, 218, 113929.

36. Abdullah, S., Murtaza, G., Asif, M., Javed, A., & Qayyum, B. (2026). Photocatalytic and photovoltaic performance of a novel two-dimensional $GaAg(PSe_3)_2$ monolayer: A first-principles study. *Chemical Physics*, 610, 113332.

37. Soler, J. M., Artacho, E., Gale, J. D., García, A., Junquera, J., Ordejón, P., & Sánchez-Portal, D. (2002). The SIESTA method for ab initio order-N materials simulation. *Journal of Physics: Condensed Matter*, 14(11), 2745–2779.

38. Perdew, J. P., Burke, K., & Ernzerhof, M. (1996). Generalized gradient approximation made simple. *Physical Review Letters*, 77(18), 3865–3868.

39. Junquera, J., Paz, Ó., Sánchez-Portal, D., & Artacho, E. (2001). Numerical atomic orbitals for linear-scaling calculations. *Physical Review B*, 64(23), 235111.

40. Matsuda, Y., Tahir-Kheli, J., & Goddard, W. A. (2010). Definitive band gaps for single-wall carbon nanotubes. *The Journal of Physical Chemistry Letters*, 1(19), 2946–2950.

41. Gracia-Espino, E. (2011). Silver-decorated nitrogen doped multiwalled carbon nanotubes as gas sensors. *PhD Thesis, IPICYT*.

42. Ouyang, Y., et al. (2024). Efficient detection of lung cancer biomarkers using functionalized transition metal dichalcogenides (MoS_2) monolayers: DFT study. *FlatChem*, 45, 100651.